Ultrafast Soft Actuators

Dietmar Hutmacher (dietmar.hutmacher@qut.edu.au)
Queensland University of Technology https://orcid.org/0000-0001-5678-2134
Benjamin Gorissen
Harvard University https://orcid.org/0000-0001-8275-7610
Simon Liponsky
QUT
Katia Bertoldi
Harvard University
Tara Shabab
QUT
Onur Bas
Queensland University of Technology https://orcid.org/0000-0001-8841-5443

Article

Keywords: soft robotics, actuators, composites, fibers, inflatable, fast

Posted Date: March 22nd, 2021

DOI: https://doi.org/10.21203/rs.3.rs-322598/v1

Abstract

The quest for an advanced soft robotic actuator technology that is fast and can execute a wide range of application-specific tasks at multiple length scales is still ongoing. Here, we demonstrate a new design strategy leveraging the concepts of miniaturisation and fibre-reinforcement to realize high-speed inflatable actuators exhibiting diverse movements. To fabricate the designs, we employ a class of additive manufacturing technology called melt electrowriting. We demonstrate 3D printing of microfibre architectures on soft elastomers with precision at unprecedently small length scales, leading to miniaturised composite actuators with highly controlled deformation characteristics. We show that owing to their small dimensions and deterministically designed fibrous networks, our actuators require extremely low amounts of fluid to inflate. We demonstrate that actuators with a length of 10 to 15mm and an inner diameter 1mm can reach their full range of motion within ~ 20ms without exploiting snapping instabilities or material non-linearities. We display the speed of our actuators by building an ultrafast, soft flycatcher.

Background

The field of soft robotics proposed the development of versatile actuators as one of the first marks on its roadmap to next-generation robotics, due to the integral role of these technologies in the function and performance of robots.[1–3] It is known that actuators determine the size, cost, power source, control mechanism, and general design of any robotic system,[4] therefore strong emphasis has been placed on the advancement of these components. Although a wide range of actuator designs have been proposed, due to their ease of operation, low cost and ability to achieve a large range of deformations, inflatable actuators have been the primary subject of interest.[5] However, these actuators are often considered too slow for most applications as their speed is limited by large inflation volumes that are needed to create deformations and the consequent large viscous forces needed to let this volume pass through narrow tubes. Several design strategies leveraging snapping instabilities,[6] material non-linearity,[7] stored elastic energy [8], as well as explosive chemical reactions [9] have been proposed to overcome this limitation. However, the functionality of the resulting inflatable actuators is highly limited as very specific considerations have to be taken into account in their design and manufacturing. Combining high actuation speeds without compromising functionality has been a major challenge and a high-speed inflatable actuator concept that can execute an extensive range of application-specific tasks is yet to be demonstrated. In this work, we aim at developing highly-functional and modular actuators that achieve high speeds.

To accomplish this goal, we investigate mechanisms that lay at the basis of nature's fast-acting structures that rely on the transportation of fluids for actuation. It has been shown that these fluid-driven actuators harness miniaturisation to achieve fast movements.[10] For instance, the Aldrovanda can close its leaves in 20ms, which is ~10 times more rapidly than the Venus flytrap, due to its significantly smaller size (approximately $1/10^{th}$ of Venus flytrap).[10] Miniaturised designs influence both the required volume

of fluid (Δ_{Volume}) that is needed to be displaced, as well as the distance it needs to travel, enabling rapid movements. Thus, we hypothesise that an analogues miniaturisation strategy can be applied to inflatable actuators (see **Figure 1**A for the schematic illustration of the concept**)**.

In addition to miniaturisation, it is essential to improve the efficiency of actuators in converting delivered fluids into fast and predictable movement. As the transportation of fluids is a fundamental problem in these systems, available volume influx has to be efficiently converted towards desired deformations by avoiding unnecessary volumetric expansions that do not contribute to the overall desired deformation (**Figure 1**A). To determine how design can influence this efficiency, we performed Finite Element (FE) simulations (see **Supplementary Text** for further information) on three common bending actuator designs (eccentric,[11] corrugated membrane [12] and fibre-reinforced [13]) and measured the inflation volume required to obtain the same degree of bending. To eliminate the effect of size, we normalised the inflation volume by L^3, where we have taken the length 'L' of the actuator as the characteristic length scale. From this analysis, we verify that the design of actuators has a major influence on bending performance. The same bending angle is reached at lower input volume for those designs that limit parasitic expansion and cross-sectional deformations. As shown in **Figure 1**B, the actuator with an eccentric design [14] first has to be inflated substantially to start bending. Then, more than 5 times Δ_{Volume} has to be delivered to achieve 100° bending when compared to the fibre-reinforced actuator design. Similarly, the formation of major bulges can be seen in the corrugated membrane actuator design, which is the hallmark of compromised performance. Based on these findings, we conclude that deterministically designed high-modulus fibre architectures are effective in converting fluid volume influx into the desired deformation. In addition to their efficiency, which is largely overlooked and yet to be exploited in the literature, fibre-reinforced actuators are proven to be highly versatile with their ability to achieve tailored motions,[1315] making them the ideal choice in our application.

While the previous analysis pointed that fibre reinforced design has the highest potential to achieve high speeds, it did not provide any information regarding the influence of the materials and/or geometry on the performance of the actuators. To investigate the dependency of inflation volume on these two factors, we conducted a series of FE analyses. We designed and simulated a fibre reinforced bending actuator consisting of double-helical fibres (both clockwise and counterclockwise) with a pitch of 390μm as well as 3 longitudinally placed fibres on one side that create bending, surrounding a hollow cylinder with an internal diameter of 1mm, a wall thickness of 0.2mm and length of 10mm. In our simulations (which were conducted using the commercial code Abaqus/Standard), we discretised the cylinder using second-order hybrid tetrahedral elements (element type: C3D10H and the fibres with 3-node quadratic beam elements (element type: B32) and actuated the models supplying incompressible fluid to the internal cavity via a fluid-cavity interaction. We modelled the material of the cylinder as incompressible neo-Hookean with the initial shear modulus m_0, while the fibres are assumed to be linear elastic with Young's modulus E and Poisson's ratio of 0.3. To begin with, we considered m_0=15kPa and E=160MPa and found that both the bending angle and pressure vary more or less linear with inflation volume (see **Figure 2**A). From the graphs of **Figure 2**A, we can identify three actuator characteristics: the inflation volume that is

needed to achieve a bending angle of 90° (ΔV_{90}), the corresponding pressure (p_{90}) and the needed energy (ΔE_{90}), which can be calculated as the area under the pressure-volume curve. For this particular actuator, ΔV_{90}=2.35µl, p_{90}=5.4kpa and ΔE_{90}=0.0064mJ. Next, we tested different initial shear moduli values ranging between 7.5kPa<m_0<120kPa for the elastomeric matrix and Young's moduli values ranging between 80Mpa<E<1.28Gpa for the fibres. As these two parameters directly influence the bending stiffness of either the cylinder ($EI=3m_0 \cdot \pi/4 \cdot (r_o^4-r_i^4)$, with r_o and r_i being the inner and outer radius of the cylinder) and the fibres ($EI=E \cdot \pi/4 \cdot r^4$, with r being the fibre radius), we can use them to assess the influence of both geometrical and material parameters on the performance of the actuators. In **Figure 2**B-D, we display these influences by plotting respectively ΔV_{90}, p_{90} and ΔE_{90} for different bending stiffnesses of either the cylinder or the surrounding fibres, where stars indicate the previously reported values. Regarding the pressure that is needed to achieve a 90° bending angle (**Figure 2**B), we can conclude that a higher pressure is needed when the bending stiffness of the cylinder increases. Surprisingly, the bending stiffness of the fibre does not have a large influence on the required input pressure levels. Regarding the inflation volume (**Figure 2**C), we found that a combination of a stiff tube with compliant fibres and a combination of stiff fibres with a compliant tube lead to higher inflation volumes than when both are stiff or compliant. We can thus conclude that there is an optimal ratio of bending stiffnesses, where fibres need to be ~15 times stiffer than the elastomeric matrix, which has been indicated by a dotted line on the figure. Lastly, The energy that is needed to bend 90° (**Figure 2**D) is dominated by and follows the same trends as the pressure dependency, which is logical since the relative pressure variation is larger than the relative volume variation while varying stiffnesses.

To create these highly dynamic bending actuators with an optimal fibre composition, we cannot rely on production processes described in the literature, as they either are incompatible with small scale production processes, [13,15–17] or lack control over fibre placements [18–20]. Therefore we developed a new manufacturing strategy that facilitates the fabrication of miniaturised composite soft actuators with precision at small length scales. We use melt electrowriting (MEW) technology,[21,22] a class of additive manufacturing system, which combines the capability of electrospinning systems to produce ultra-fine fibres (fibre diameters between 1-50µm) with the design freedom of 3D printing. In this automated process, we apply a thin layer of uncured soft silicone-based elastomer on the rotational collector of our MEW system. By using a rod integrated into our MEW device, we move the stage in x-direction back and forwards with an elastomer and create a thin, uniform layer of the silicone-based tubular structure. We then start melt electrowriting of fibrous network designs on this partially-cured silicone tube to achieve enhanced bonding between the fibres and matrix material. (see **Figure S1** and **Movie S1** for the schematic illustration and video of the fabrication process, respectively). After the completion of the 3D printing process, we allow the silicone to fully-cure and connect the actuators to a pressure source after sealing their tip.

As demonstrated in **Figure 3**, we successfully fabricated a miniaturised bending actuator with an internal void diameter of 1mm, length of 10mm and a wall thickness of 0.2mm using our manufacturing technique (see **Figure S2** for the technical drawing). The scanning electron micrograph (**Figure 3**A) shows

the accurate placement of the fibres as well as their good continuity and consistency (see **Table S1** for the detailed characterisation of the dimensions of the fabricated actuator). We selected the constituent materials of this actuator in accordance with the established principles depicted in **Figure 2**. As our findings indicate that the use of soft matrix materials reduces the required actuation energy, we applied the softest grade silicone within the product family of a widely used elastomer (Ecoflex with a shore hardness of 00-10). For the fabrication of the fibre phase, we preferred polycaprolactone (PCL) due to its excellent rheological properties and processability via MEW process as well favourable mechanical properties (elastic modulus of 320MPa), leading to an actuator with a fibre-to-matrix bending stiffness ratio of ~7.5. Although this ratio is smaller than the identified ideal ratio, our simulations suggest that this actuator (internal diameter of 1mm, and length of 10mm) require Δ_{Volume} of 2.3559µl to achieve 90° bending, which is marginally higher than that of an actuator built with materials having a bending stiffness ratio of 15 (Δ_{Volume} of 2.3143µl). Overall, this material combination yielded high performant bending actuators that are also easy to manufacture, handle and characterise as demonstrated in **Figure 3**.

After pressurizing the actuator, we indeed observed the intended large bending movements with minimum parasitic deformations (see **Figure 3**A) (see **Figure S6** for a bending actuator without helical fibres exhibiting large parasitic deformations). **Figure 3**B shows the magnitude of the deformations achieved by the actuator at given air pressure both experimentally and as computed by means of FE modelling (see **Movie S2**). By downscaling the dimensions to diameter 1mm we were able to fabricate bending actuators that reach full stroke (270°) when inputting only volumes of less than 7.5µl. Furthermore, by modelling the volumetric expansion of our actuator using FEM, we see radially restricted actuators are characterized by a linear displacement-volume relationship. This means that the input volume is efficiently redirected towards only one spatial dimension, giving a leveraging effect for fast actuation. To confirm this, we have tested our bending actuators under a high-frequency pneumatic input (on-off), where the input air pressure was adjusted such that a full stroke was reached at the end of the cycle (see **Figure 3**C and **Figure S8** for details). We were able to achieve an actuation frequency reaching 30Hz, where complete bending and recovery to initial state takes place within ~30ms (see **Movie S7**). Further, we see that the dynamics are limited by the deflation part of the cycle. In contrast to inflation where we can adjust the input pressure to reach full stroke quicker, the deflation of the actuator is limited by an atmospheric back-pressure, resulting in a maximum actuation frequency of 30 Hz.

The presented methodology of combining miniaturisation with a fibre reinforcement design showed to be a highly successful pathway of creating highly dynamic actuators. However, this methodology is not limited to only bending deformations. Using the fabrication freedom of additive manufacturing, we can deposit fibres at arbitrary positions and orientations, as displayed in **Figure 4**. The fibre architectures that give rise to the unique deformation of these actuators are displayed using SEM images, where for twining we combined helical fibres with three grouped eccentric fibres, for extending we remove the eccentric fibres, and for contracting we only use eccentric fibres that are evenly spaced. Further, these actuators were dynamically tested, resulting in a maximum actuation frequency of 20Hz for twining, 30Hz for

contraction and 30Hz for elongation actuators (see **Movie SI8-10** for high-speed actuation videos, **Figure SI3-5** for technical drawings of the actuators and **Figure SI7** for detailed characterisation results).

Finally, to demonstrate the performance of our actuators, we applied them in a setting where speed, small scale and compliance are of the utmost importance: catching of a fly without killing it. Towards this goal, we developed a soft robotic flycatcher (**Figure 5**B). The flycatcher consists of three bending actuators that are placed in a triangular pattern around a 3D-printed base with a central cylindrical target area (see **Supplementary Text** for further information and **FigureS10** for the technical drawing). When a fly is detected, we apply air pressure to the three bending actuators using a syringe, rapidly closing the trap, successfully catching the fly in the process (see **Figure 5**B and **Movie S11**). Furthermore, by combining various actuator designs in a linear or parallel manner, a wide range of miniaturized compliant devices such as actuators that transform into very complex shapes (**Movie S12**) and endoscopic systems that are able to navigate through complex and constrained environments (**Movie S13**) can be developed.

In conclusion, by enabling the seamless implementation of the concepts of fibre-reinforcement to control volumetric expansion and miniaturisation, we were able to create a wide variety of actuator deformations with the application of only a few microliters of actuation volume. As volume flux is typically the limiting factor for speed, we were able to create high dynamic motions (up to ~30Hz) using standard pressure regulators. Our additive manufacturing-based automated manufacturing platform allowed us to down-scaling the dimensions of fibre-reinforced actuators without compromising their functionality. Such actuators that operate with low-volume and -pressure fluids and exhibit minor volumetric changes are also highly advantageous in applications where space of operation is limited. In the present study, we focused our investigation on inflatable elastomers. Yet, in future studies, alternative actuation methods can be explored by incorporating different matrix materials that respond to alterations in osmotic conditions, pH, magnetic fields or temperatures. The deformation of this type of soft matter can be guided via our 3D-printed fibrous network, which may unlock new research directions towards the development of a new generation of soft smart materials, actuators and robots.

Methods

Fabrication of soft actuators:

The fabrication process of the actuators starts with the application of a viscous platinum-catalysed silicone (Ecoflex 00-10, Smooth-On Inc., USA) onto the printing collector (rod) of the MEW device. First, Parts A and B of the silicon were mixed and stirred thoroughly for 2min (1A:1B by volume), drawn into a positive displacement pipette and applied to the rotating printing collector after 18mins until a volume sufficient for a wall thickness of ~200µm is deposited. With the aid of a 0.5mm diameter metal rod attached to the print head of the MEW system that lightly touches the rotating printing collector, the partially-cured silicon was uniformly dispersed by moving the translational linear stage of the system back and forth along the main axis of the printing collector for ~3 mins while it was rotating.

Subsequently, the printing process of the fibrous network onto the partially-cured silicon was commenced (see **Movie S1** for the fabrication process).

For the preparation of the MEW device, first, medical-grade polycaprolactone pellets (Purasorb PC 12, Purac Biomaterials, the Netherlands) were placed in a syringe and heated to a temperature of 80 °C in the extrusion head of the device. After allowing the polymer to reach a steady molten state (~10 mins), air pressure of 1.5 bar was applied to the syringe using an electro-pneumatic pressure regulator (ITV0030, SMC, Japan) to extrude the molten polymer through a 23G needle. During the extrusion, a voltage of 4.9 – 5 kV was applied to the needle that leads to the formation of a fine, stable polymeric jet. The printing collector-to-needle distance was set to 3mm, and the jet was deposited onto the collector at a speed of 165mm/min (combined translational (linear stage) and tangential speed (rotational stage)). MEW is a computer-aided manufacturing technique which utilises programs written in G-Code-based numerical controlling language (see **Table S2**). The fibrous networks were printed onto the partially-cured silicone to enhance the adhesion between the matrix material and fibres. After the completion of the printing process, the silicone was left to fully-cure for 2 hours. The actuators were then peeled off the rods with ethanol aiding as a lubricant. The actuators were mounted to a pressure source after sealing their tip with air-curing silicone (Sil-Poxy, Smooth-On Inc., USA).

Characterisation of the soft pneumatic actuators:

Scanning electron microscopy

The micrographs of the actuators and fibrous networks were acquired using a Tescan MIRA3 scanning electron microscope (SEM). Samples were first gold-coated for 75 seconds at 30mA (Leica EM-SCD005 gold sputter coater, Wetzlar, Germany) before imaging.

Characterization of the movement in response to pressure

The actuators were driven with air using a custom-made syringe pump, and their static images, as well as their videos, were acquired using a handheld digital microscope (Dino-Lite Edge 5MP, AnMo Electronics Corporation). The pressure values within the system were measured using a pressure sensor (HSCDANN005PGAA5, Honeywell Sensing and Productivity Solutions), which is placed next to the actuators.

High-frequency and rapid actuation tests (dynamic)

For the high-frequency actuation tests, a pneumatic system (Performus VII, Nordson Electron Fusion Devices, Inc) controlled by an external microcontroller was used. The pressure of the delivered air was adjusted for each actuator type to enable their full range of motion within the duration of each actuation cycle (see **Figure S8**). At higher frequencies (> ~10Hz), high-pressure values exceeding the regular actuation requirements of the actuators was set as the response of the system was found to be slow to reach the desired levels in the given time if high-pressure values are not used. The pressure values were

measured using a pressure sensor (HSCDANN005PGAA5, Honeywell Sensing and Productivity Solutions), which was placed at the actuator-end of the experimental setup.

Measurement of the volumetric expansion (static)

The volumetric expansion of the actuators after their actuation was quantified by measuring the amount of fluid (H_2O) that is delivered with a positive displacement pipette. The actuators were submerged in water during the tests to avoid the deformations caused by the weight of the supplied water.

Simulations:

The response of our actuators upon inflation was modelled using the Finite Element (FE) method, using the commercial package ABAQUS (2019/Standard). In the fibre actuator analyses, the silicone rubber was modelled as an incompressible Neo-Hookean hyperelastic material model with initial shear modulus μ_0 of 30kPa. The fibres were modelled as a linear elastic material with Young's modulus E of 320 MPa and a Poisson ratio n of 0.3. The cylindrical rubber tube was discretised using 3D tetrahedral hybrid solid elements (element code C3D10H), while the fibres were discretised using 3-node quadratic beam elements (element code B32). The fibres and cylindrical tube are meshed separately and connected to each other using a tie constraint that allows no slipping of the fibres relative to the tube. We pressurize the actuators by supplying incompressible fluid to the internal cavity while monitoring the pressure inside and simulate the quasi-static behaviour using a static solver.

Declarations

Acknowledgements

The authors thank Mr Pawel Mieszczanek and Mr Aaron Foster for their assistance in the experiments. This work was financially supported by the Australian Research Council Industrial Transformation Training Centre (external ref: IC160100026, Queensland University of Technology)

Author contributions

O.B. initiated and conceived the research, performed experiments, analysed data and drafted the manuscript; B.G. performed the simulations, contributed to the design of the study, interpretation of the data and writing of the manuscript; S.L. contributed to the design, fabrication and characterisation of the soft actuators; T.S. performed SEM imaging; K.B. and D.W.H provided direction and edited the manuscript.

Competing interests

The authors declare no competing interests.

Supplementary information

The online version contains supplementary material.

References

1. Laschi, C., Mazzolai, B. & Cianchetti, M. Soft robotics: Technologies and systems pushing the boundaries of robot abilities. *Sci. Robot.***3690**, eaah3690 (2016).
2. Ricotti, L. *et al.* Biohybrid actuators for robotics: A review of devices actuated by living cells. *Sci. Robot.***2**, eaaq0495 (2017).
3. Yang, G.-Z. *et al.* The grand challenges of *Science Robotics*. *Sci. Robot.***3**, eaar7650 (2018).
4. Alici, G. Softer is Harder: What Differentiates Soft Robotics from Hard Robotics? *MRS Adv.* 1–12 (2018). doi:10.1557/adv.2018.159
5. Gorissen, B. *et al.* Elastic Inflatable Actuators for Soft Robotic Applications. *Adv. Mater.***29**, 1–14 (2017).
6. Gorissen, B., Melancon, D., Vasios, N., Torbati, M. & Bertoldi, K. Inflatable soft jumper inspired by shell snapping. *Sci. Robot.***5**, eabb1967 (2020).
7. Baumgartner, R. *et al.* A Lesson from Plants: High-Speed Soft Robotic Actuators. *Adv. Sci.***7**, (2020).
8. Pal, A., Goswami, D. & Martinez, R. V. Elastic Energy Storage Enables Rapid and Programmable Actuation in Soft Machines. *Adv. Funct. Mater.***30**, 1–9 (2020).
9. Shepherd, R. F. *et al.* Using explosions to power a soft robot. *Angew. Chemie - Int. Ed.***52**, 2892–2896 (2013).
10. Skotheim, J. M. & Mahadevan, L. Plant science: Physical limits and design principles for plant and fungal movements. *Science (80-.).***308**, 1308–1310 (2005).
11. Gorissen, B., De Volder, M., De Greef, A. & Reynaerts, D. Theoretical and experimental analysis of pneumatic balloon microactuators. *Sensors Actuators, A Phys.***168**, 58–65 (2011).
12. Mosadegh, B. *et al.* Pneumatic networks for soft robotics that actuate rapidly. *Adv. Funct. Mater.***24**, 2163–2170 (2014).
13. Connolly, F., Polygerinos, P., Walsh, C. J. & Bertoldi, K. Mechanical Programming of Soft Actuators by Varying Fiber Angle. *Soft Robot.***2**, 26–32 (2015).
14. Shapiro, Y., Wolf, A. & Gabor, K. Bi-bellows: Pneumatic bending actuator. *Sensors Actuators, A Phys.***167**, 484–494 (2011).
15. Connolly, F., Walsh, C. J. & Bertoldi, K. Automatic design of fiber-reinforced soft actuators for trajectory matching. *Proc. Natl. Acad. Sci.***114**, 51–56 (2017).
16. Galloway, K. C., Polygerinos, P., Walsh, C. J. & Wood, R. J. Mechanically programmable bend radius for fiber-reinforced soft actuators. *2013 16th Int. Conf. Adv. Robot. ICAR 2013* 1–6 (2013). doi:10.1109/ICAR.2013.6766586
17. Kim, S. Y. *et al.* Reconfigurable soft body trajectories using unidirectionally stretchable composite laminae. *Nat. Commun.***10**, 3464 (2019).

18. Cappello, L. *et al.* Exploiting Textile Mechanical Anisotropy for Fabric-Based Pneumatic Actuators. *Soft Robot.***5**, 662–674 (2018).
19. Sinatra, N. R. *et al.* Ultragentle manipulation of delicate structures using a soft robotic gripper. *Sci. Robot.***4**, eaax5425 (2019).
20. Sinatra, N. R., Ranzani, T., Vlassak, J. J., Parker, K. K. & Wood, R. J. Nanofiber-reinforced soft fluidic micro-actuators. *J. Micromechanics Microengineering***28**, 084002 (2018).
21. Brown, T. D., Dalton, P. D. & Hutmacher, D. W. Direct writing by way of melt electrospinning. *Adv. Mater.***23**, 5651–5657 (2011).
22. Wunner, F. M. *et al.* Melt Electrospinning Writing of Highly Ordered Large Volume Scaffold Architectures. *Adv. Mater.***1706570**, 1706570 (2018).
23. Yuk, H. *et al.* Hydraulic hydrogel actuators and robots optically and sonically camouflaged in water. *Nat. Commun.***8**, 14230 (2017).
24. Chou, C. P. & Hannaford, B. Measurement and modeling of McKibben pneumatic artificial muscles. *IEEE Trans. Robot. Autom.***12**, 90–102 (1996).
25. Suzumori, K., Iikura, S. & Tanaka, H. Development of flexible microactuator and its applications to robotic mechanisms. in *Proceedings - IEEE International Conference on Robotics and Automation***2**, 1622–1627 (1991).
26. Polygerinos, P., Wang, Z., Galloway, K. C., Wood, R. J. & Walsh, C. J. Soft robotic glove for combined assistance and at-home rehabilitation. *Rob. Auton. Syst.***73**, 135–143 (2015).
27. Gong, X. *et al.* Rotary Actuators Based on Pneumatically Driven Elastomeric Structures. *Adv. Mater.***28**, 7533–7538 (2016).
28. Takemura, K., Yokota, S. & Edamura, K. A micro artificial muscle actuator using electro-conjugate fluid. *Proc. - IEEE Int. Conf. Robot. Autom.***2005**, 532–537 (2005).
29. Yamaguchi, A., Takemura, K., Yokota, S. & Edamura, K. A robot hand using electro-conjugate fluid. *Proc. - IEEE Int. Conf. Robot. Autom.* 5923–5928 (2011). doi:10.1109/ICRA.2011.5979691
30. Correll, N., Önal, Ç. D., Liang, H., Schoenfeld, E. & Rus, D. Soft Autonomous Materials—Using Active Elasticity and Embedded Distributed Computation BT - Experimental Robotics: The 12th International Symposium on Experimental Robotics. in (eds. Khatib, O., Kumar, V. & Sukhatme, G.) 227–240 (Springer Berlin Heidelberg, 2014). doi:10.1007/978-3-642-28572-1_16
31. Gorissen, B., De Volder, M. & Reynaerts, D. Pneumatically-actuated artificial cilia array for biomimetic fluid propulsion. *Lab Chip***15**, 4348–4355 (2015).
32. Marchese, A. D., Katzschmann, R. K. & Rus, D. A Recipe for Soft Fluidic Elastomer Robots. *Soft Robot.***2**, 7–25 (2015).
33. Sasaki, D., Noritsugu, T. & Takaiwa, M. Development of active support splint driven by pneumatic soft actuator (ASSIST). *Proc. - IEEE Int. Conf. Robot. Autom.***2005**, 520–525 (2005).
34. Kato, N. *et al.* Elastic Pectoral Fin Actuators for Biomimetic Underwater Vehicles BT - Bio-mechanisms of Swimming and Flying. in (eds. Kato, N. & Kamimura, S.) 271–282 (Springer Japan,

2008).
35. Tolley, M. T. *et al.* A Resilient, Untethered Soft Robot. *Soft Robot.***1**, 213–223 (2014).
36. Shepherd, R. F. *et al.* Multigait soft robot. *Proc. Natl. Acad. Sci. U. S. A.***108**, 20400–20403 (2011).
37. Konishi, S., Kawai, F. & Cusin, P. Thin flexible end-effector using pneumatic balloon actuator. *Sensors Actuators, A Phys.***89**, 28–35 (2001).
38. Hines, L., Petersen, K., Lum, G. Z. & Sitti, M. Soft Actuators for Small-Scale Robotics. *Adv. Mater.***29**, (2017).
39. Schaffner, M. *et al.* 3D printing of robotic soft actuators with programmable bioinspired architectures. *Nat. Commun.***9**, 878 (2018).
40. Maccurdy, R., Katzschmann, R., Kim, Y. & Rus, D. Printable hydraulics: A method for fabricating robots by 3D co-printing solids and liquids. *Proc. - IEEE Int. Conf. Robot. Autom.***2016-June**, 3878–3885 (2016).
41. Peele, B. N., Wallin, T. J., Zhao, H. & Shepherd, R. F. 3D printing antagonistic systems of artificial muscle using projection stereolithography. *Bioinspiration and Biomimetics***10**, (2015).
42. Zolfagharian, A. *et al.* Sensors and Actuators A : Physical Evolution of 3D printed soft actuators. *Sensors Actuators A. Phys.***250**, 258–272 (2016).
43. Tawk, C., Panhuis, M. in het, Spinks, G. M. & Alici, G. Bioinspired 3D Printable Soft Vacuum Actuators. *Soft Robot.***5**, 685–694 (2018).
44. Wallin, T. J., Pikul, J. & Shepherd, R. F. 3D printing of soft robotic systems. *Nat. Rev. Mater.***3**, 84–100 (2018).
45. Skylar-Scott, M. A., Mueller, J., Visser, C. W. & Lewis, J. A. Voxelated soft matter via multimaterial multinozzle 3D printing. *Nature***575**, 330–335 (2019).

Figures

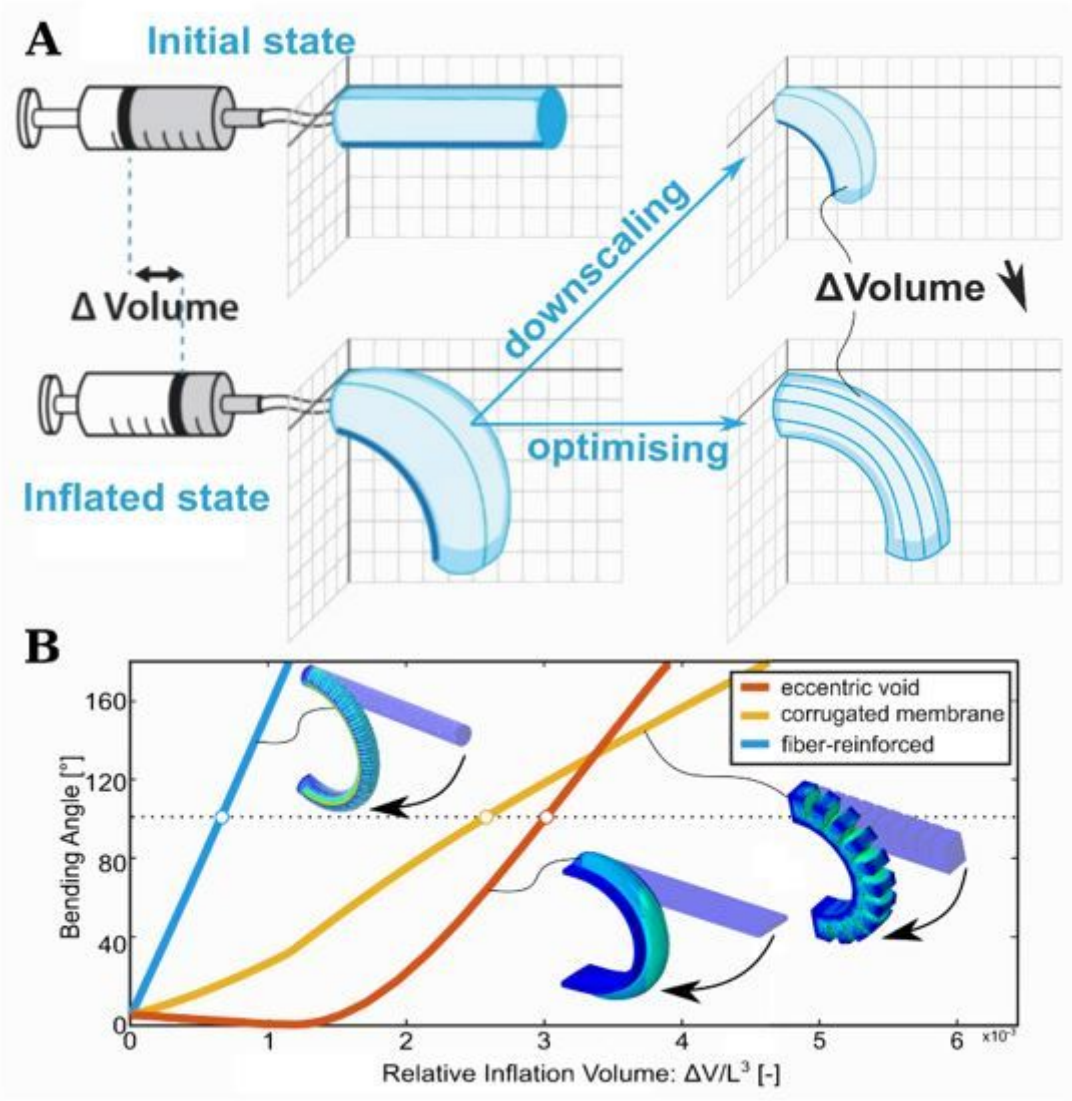

Figure 1

Design rationale for achieving high-speed soft actuators. (A) Schematic illustration demonstrating the concept of fibre reinforcement and miniaturisation to reduce ΔVolume needed for actuation, which is critical for achieving high-speed actuation via regular pressure suppliers. (B) The influence of actuator design on the performance (capability of converting volume inputs into desired deformations). The figure indicates that certain actuator designs exhibit less parasitic deformations when inflated and require less volume input to achieve the same degree of bending.

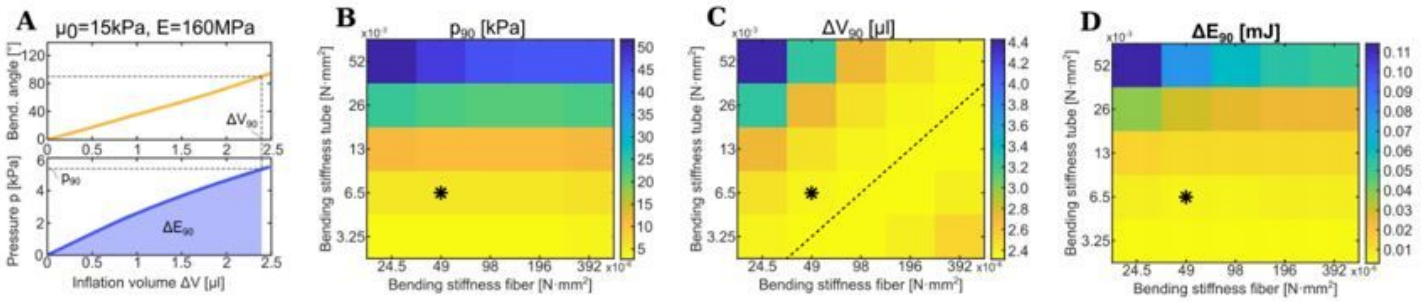

Figure 2

Parameter variation study. (A) Simulated action characteristics for an actuator composed out of rubber with 0=15kPa and fibres with E=160MPa. (B) The pressure that is needed to achieve a bending angle of 90° for changing bending stiffnesses of the fibres and the elastomeric tube. (C) The inflation volume that is needed to achieve a bending angle of 90° for changing bending stiffnesses of the fibres and the elastomeric tube. The dotted line depicts optimal actuators that require a minimum in inflation volume. (D) The energy that is needed to achieve a bending angle of 90° for changing bending stiffnesses of the fibres and the elastomeric tube. The stars are indicative of the performance of the actuator displayed in (A).

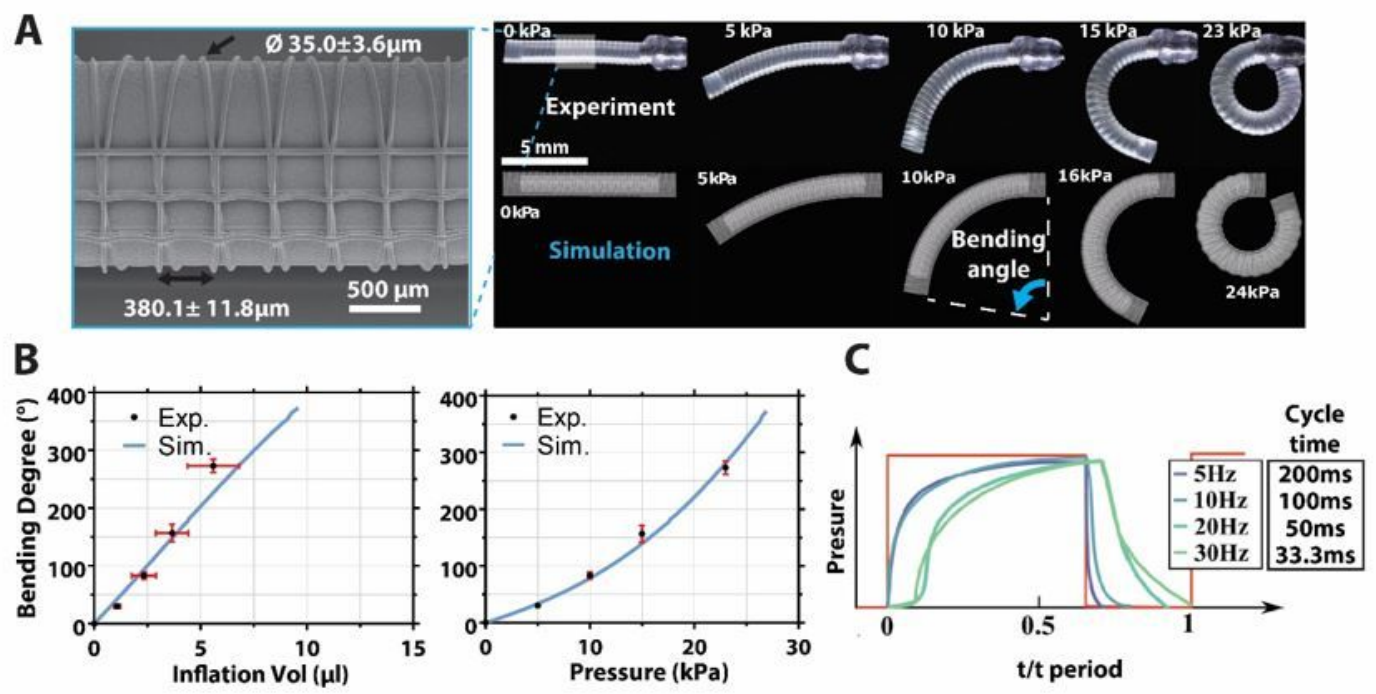

Figure 3

Characterisation of the performance of bending actuators. (A) Deformation behaviour of a representative bending actuator in comparison to the deformations obtained via simulations. Scanning electron microscopy image of the actuator is also shown. (B) Graphs of inflation volume vs deformation and input

pressure vs deformation obtained via experiments (n=3) and simulations. (C) Air pressure values measured while characterising the actuation performance of the bending actuators at different actuation frequencies (5, 10, 20 to 30Hz). At frequencies > ~10Hz, pressure values exceeding the regular actuation pressure requirements of the actuators were applied to be able to reach the desired pressure levels within each actuation cycle (see Figure S8 for exact values). The duty cycle was kept constant (on-to-off duration ratio of 2) for all the experiments.

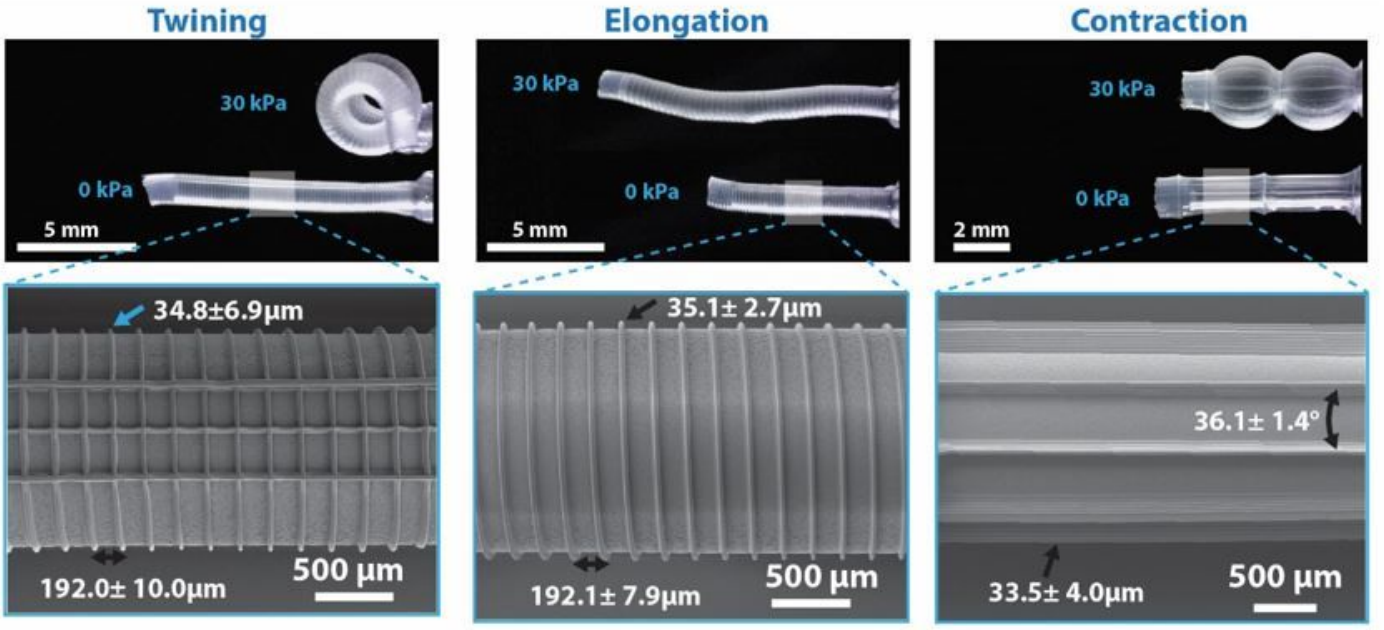

Figure 4

Miniaturised soft actuators exhibiting various movements. Representative twining-, elongation- and contraction-type actuators with their scanning electron micrographs. To benchmark these actuators, we have collected the dynamic data (time to complete an actuation cycle) of inflatable actuators from the literature and plotted it against their length scale (see Figure 5A).11,12,31–37,23–30 As illustrated, research efforts towards miniaturisation have been focused on actuators with bending and extending deformations, due to a lack of advanced manufacturing techniques that are needed to create other more complex deformations.38 Actuators with other deformation modes are typically found at larger scales,3915 where limited dynamic data is provided for them. Whereas we showed that additive manufacturing can create pathways for high dynamic actuators, typically these technologies are not well suited for miniaturisations or combining multiple materials.39–45. Therefore, as shown in Figure 5A, the majority of the miniaturised actuators were fabricated via various moulding techniques and are limited to only one actuation mode. As demonstrated, our MEW-based fabrication method provides large design flexibility, giving rise to an increase in the design space of miniaturised actuators. We identified that our actuators are not only among the fastest in their class (actuators based on forced inflation) but also outperform their counterparts with respect to achievable deformation diversity (Figure 5A). Furthermore, the collected data also points to the same conclusion as Nature -smaller systems are able to reach higher actuation speeds.

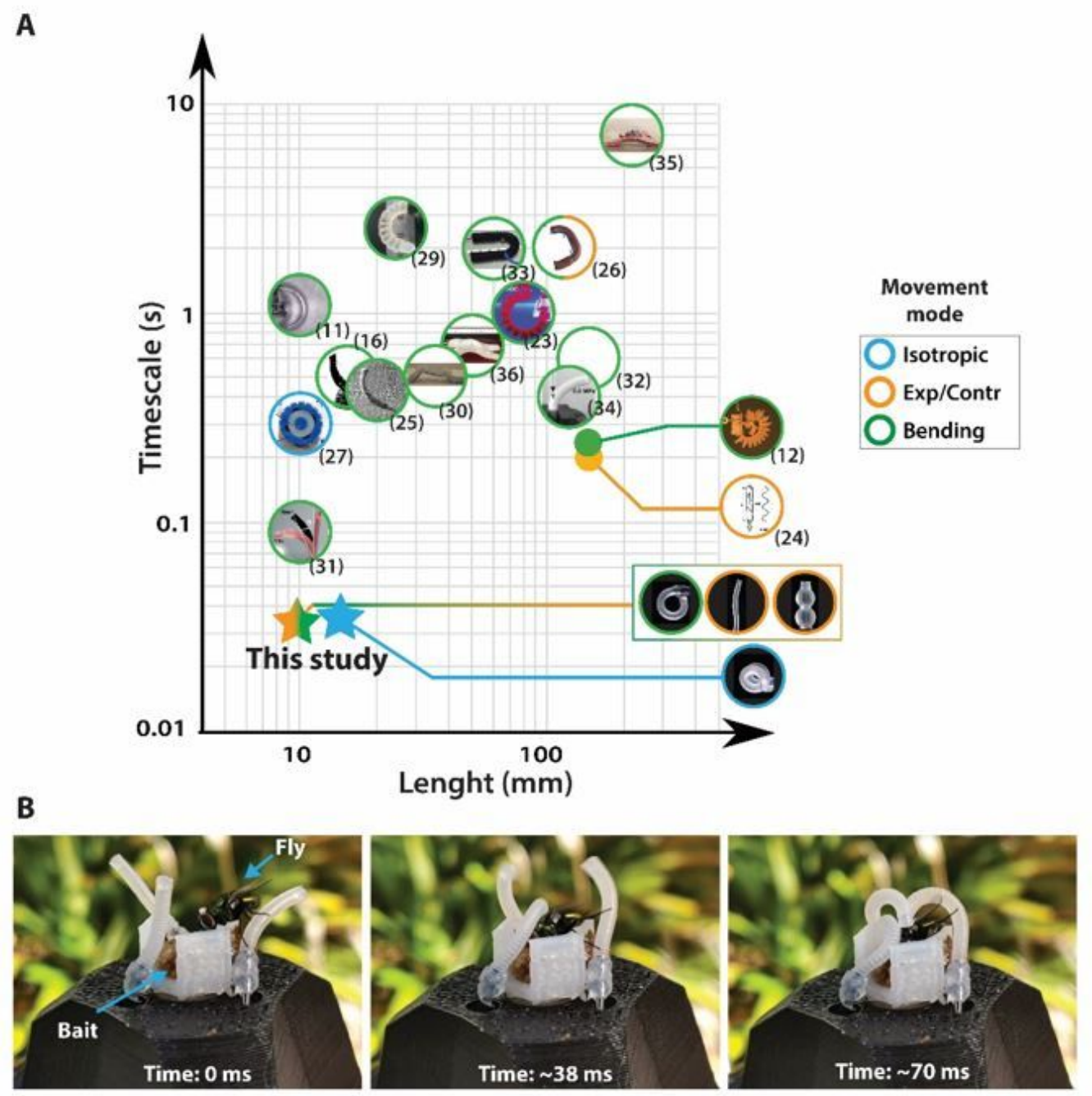

Figure 5

(A) Actuation speed vs size plot of soft inflatable actuators from published studies benchmarked against the actuators developed in our labs. The mode of deformation of the actuators is classified with colour codes. (B) We demonstrate the speed of our soft actuators via the built of a flycatcher. The design is based on a 3D-printed base (black part) and three bending-type actuators that catch the fly (Lucilia cuprina).

Supplementary Files

This is a list of supplementary files associated with this preprint. Click to download.

- MovieS4.ElongationTwistingactuator.mp4
- MovieS9.HighfrequencyactuationElongationinslowmo.mp4
- SupportingInfoNatComm.docx
- MovieS12.WritingQUTlogo.mp4
- MovieS2.Bendingactuator.mp4
- MovieS13.Endoscopicdevicenavigatingwithinchannels.mp4
- MovieS1.Fabricationoffibrereinforcedsoftactuators.mp4
- MovieS10.HighfrequencyactuationContractioninslowmo.mp4
- MovieS5.Contractionactuator.mp4
- MovieS6.Inflatingsilicone.mp4
- MovieS7.HighfrequencyactuationBendinginslowmotion.mp4
- SupportingInfoNatComm.docx
- MovieS3.Twiningactuator.mp4
- MovieS11.Flycatcherslowmotion.mp4
- MovieS8.HighfrequencyactuationTwininginslowmotion.mp4